
DyKAF: Dynamical Kronecker Approximation of the Fisher Information Matrix for Gradient Preconditioning

Nikolay Yudin*
HSE University
neyudin@edu.hse.ru

Ekaterina Grishina*
HSE University

Andrey Veprikov*
Basic Research of Artificial
Intelligence Laboratory (BRAIn Lab)

Alexandr Beznosikov
Basic Research of Artificial
Intelligence Laboratory (BRAIn Lab)
Innopolis University

Maxim Rakhuba
HSE University

Abstract

Recently, optimizers that explicitly treat weights as matrices, rather than flattened vectors, have demonstrated their effectiveness. This perspective naturally leads to structured approximations of the Fisher matrix as preconditioners, where the matrix view induces a Kronecker-factorized form that enables memory-efficient representation. However, constructing such approximations both efficiently and accurately remains an open challenge, since obtaining the optimal factorization is resource-intensive and practical methods therefore rely on heuristic design choices. In this work, we introduce a novel approach that leverages projector-splitting integrators to construct effective preconditioners. Our optimizer, **DyKAF** (Dynamical Kronecker Approximation of the Fisher Matrix), consistently improves the Fisher matrix approximation quality. Experiments on large language model pre-training and fine-tuning demonstrate that **DyKAF** outperforms existing optimizers across a range of evaluation metrics.

second-order methods estimate the full curvature of the loss surface through approximations of the Hessian matrix and thereby enable faster convergence (Semenov et al., 2025b).

However, exact computation and storage of the Hessian matrix remains infeasible for models with billions of parameters (Hernández-Cano et al., 2025), which motivates ongoing research into scalable and accurate approximations. One effective approach is natural gradient descent (Amari, 1998), which uses the Fisher information matrix (see Equation 3 in Section 4) as an approximation of the Hessian.

The empirical Fisher information matrix, often computed independently for each neural network layer, provides a practical (Martens, 2020; Frantar et al., 2021; Wu et al., 2024) and theoretically grounded surrogate for the full Hessian under certain conditions (Kunstner et al., 2019; Semenov et al., 2025a).

Nevertheless, even when restricted to layerwise blocks, the Fisher information matrix remains prohibitively large, making both its storage and inversion computationally expensive. To address this, several approximations have been proposed, most notably the Kronecker-Factored Approximate Curvature (K-FAC) method (Martens and Grosse, 2015), as well as more recent related optimizers such as Shampoo (Gupta et al., 2018) and SOAP (Vyas et al., 2024). These approaches treat model parameters as matrices and leverage Kronecker factorization to reduce computational complexity while retaining meaningful curvature information. For a comprehensive overview of the Kronecker-Factored methods, we refer the reader to Section 7.

A fundamental limitation of Kronecker approximation methods is the inability to compute optimal factors without the full Fisher matrix. Consequently, these methods often inaccurately approximate the true Hessian, as shown in Figure 1. In this small-scale experiment, we evaluate Hessian approximation accuracy in a classification setup, where the Hessian is analytically computable (see details in Appendix A). This setup allows a direct comparison between the preconditioners

1 Introduction

Efficient optimization is crucial for training deep models, both during pretraining on large datasets and fine-tuning for specific tasks (Goodfellow et al., 2016; Team et al., 2025; Parthasarathy et al., 2024). Various optimization methods like classical SGD (Rumelhart et al., 1986) or recent Muon (Jordan et al., 2024) rely primarily on gradient information and do not approximate curvature of the loss function. The widely adopted Adam optimizer (Kingma and Ba, 2014) takes it into account by applying a diagonal preconditioning that scales each parameter independently. More advanced

*Equal contribution

of state-of-the-art methods like SOAP (Vyas et al., 2024) and our proposed optimizer, DyKAF (Algorithm 3, Section 5).

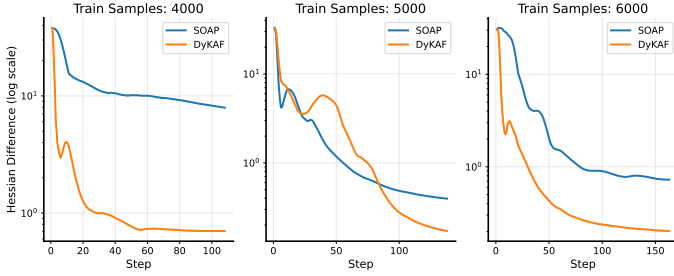


Figure 1: Comparison of Hessian approximation in the controlled environment. The Frobenius norm of the difference between the Hessian and its approximations by SOAP and DyKAF (Algorithm 3) is shown for varying training sample sizes. Our algorithm achieves consistently better approximation accuracy.

An imprecise approximation of the Fisher information matrix in existing methods can limit the effectiveness of gradient preconditioning. This work aims to improve the accuracy of Kronecker product updates via the so-called projector-splitting scheme for dynamical low-rank approximation. Our main contributions are:

- We propose an algorithm to maintain the Kronecker product approximation of the Fisher matrix using projector-splitting integrator (Lubich and Oseledets, 2014; Ceruti et al., 2022). We incorporate this approach into SOAP optimizer by modifying the update formulas for Kronecker factors (see Algorithm 3). These updates add negligible overhead (see Algorithm 2) and integrate seamlessly into the SOAP framework, using the same hyperparameters (see Section 6.2).
- We provide a theoretical analysis comparing the accuracy of the dynamical Kronecker approximation of Fisher matrix and the update formula of Shampoo and SOAP (see Section 4). Our theoretical findings are supported by empirical evaluations.
- We conduct a thorough evaluation of our method on language model fine-tuning (Section 6.1) and pretraining (Section 6.2) tasks showing a performance improvement in comparison with the state-of-the-art alternatives.

2 Notation and Background

2.1 Preliminaries

In this section, we recap some well-known facts from linear algebra, see (Golub and Van Loan, 2013). Note that we will use row-major index ordering as in Pytorch. Further in the text, $\|A\| = \sqrt{\sum_{ij} A_{ij}^2}$ denotes the Frobenius norm.

Definition 1. For any square matrix $A \in \mathbb{R}^{n \times n}$, let $\text{off}(A) \in \mathbb{R}^{n \times n}$ be the matrix obtained by subtracting the diagonal part of A :

$$\text{off}(A) := A - \text{diag}(A).$$

Definition 2. For any matrix $A \in \mathbb{R}^{m \times n}$, let $A^{\circ\alpha}$ denote a Hadamard (elementwise) power of a matrix:

$$(A^{\circ\alpha})_{ij} = A_{ij}^\alpha, \quad \forall i, j.$$

Definition 3. Let $\text{vec}(X) \in \mathbb{R}^{mn}$ denote a vector obtained by “stacking” rows of the matrix $X \in \mathbb{R}^{m \times n}$:

$$\text{vec}(X) := \begin{bmatrix} X[0, :]^\top \\ \vdots \\ X[n-1, :]^\top \end{bmatrix}.$$

It is well known that for $B \in \mathbb{R}^{m_1 \times n_1}$, $C \in \mathbb{R}^{m_2 \times n_2}$, and $X \in \mathbb{R}^{n_1 \times n_2}$, the following identity holds:

$$Y = BXC^\top \Leftrightarrow \text{vec}(Y) = (B \otimes C)\text{vec}(X), \quad (1)$$

where \otimes denotes the Kronecker product. Similarly to the definition of the vectorization operation, let us define an inverse operation called matricization.

Definition 4. For a vector $x \in \mathbb{R}^{mn}$ let the matricization operator $\text{Mat}(x) \in \mathbb{R}^{m \times n}$ denote a matrix which is obtained by “packing” x into an m -by- n matrix in the row-major order:

$$\text{Mat}(x) := \begin{bmatrix} x[0:n]^\top \\ \dots \\ x[in:(i+1)n]^\top \\ \dots \\ x[(m-1)n:mn]^\top \end{bmatrix}.$$

Let $A \in \mathbb{R}^{m_1 m_2 \times n_1 n_2}$. The Nearest Kronecker Product (NKP) problem reads as:

$$\|A - B \otimes C\| \rightarrow \min_{B, C}, \quad (2)$$

where $B \in \mathbb{R}^{m_1 \times n_1}$ and $C \in \mathbb{R}^{m_2 \times n_2}$. This problem can be solved using a rearranged version of A .

Definition 5. Let us define a rearrangement operator $\mathcal{R}(\cdot)$, which rearranges elements from $A \in \mathbb{R}^{m_1 m_2 \times n_1 n_2}$ into $\mathcal{R}(A) \in \mathbb{R}^{m_1 n_1 \times m_2 n_2}$ in the following way:

$$\mathcal{R}(A)[m_2 i + i', n_2 j + j'] = A[n_1 i + j, n_2 i' + j'].$$

The rearrangement operator has several useful properties. In particular, it maps Kronecker product into a rank-1 matrix:

$$\mathcal{R}(B \otimes C) = \text{vec}(B)\text{vec}(C)^\top.$$

This property of the rearrangement operator helps to obtain the following fact.

Proposition 1 (Golub and Van Loan (2013)). The NKP approximation problem 2 is equivalent to finding the best rank-1 approximation to $\mathcal{R}(A)$:

$$\|\mathcal{R}(A) - \text{vec}(B)\text{vec}(C)^\top\| \rightarrow \min_{B, C}.$$

Thus, the proposition above allows us to approach the NKP problem for a certain matrix $A \in \mathbb{R}^{mn \times mn}$ as a rank-1 approximation of the rearranged matrix $\mathcal{R}(A) \in \mathbb{R}^{m^2 \times n^2}$.

3 The Fisher Information Matrix Angle of Shampoo and SOAP

Let us first define the empirical Fisher information matrix $F_t \in \mathbb{R}^{mn \times mn}$ for a layer with a weight matrix $W \in \mathbb{R}^{m \times n}$ as

$$F_t := \sum_{i=1}^t \text{vec}(G_i) \text{vec}(G_i)^\top, \quad (3)$$

where $G_i \in \mathbb{R}^{m \times n}$ is the gradient with respect to the layer W on the i -th optimization step. Note that in this work we consider only matrix-shaped parameters.

Recent works (Martens and Grosse, 2015; Gupta et al., 2018; Vyas et al., 2024) have investigated methods to approximate the Fisher matrix with a Kronecker product of two smaller matrices $L_t \in \mathbb{R}^{m \times m}$, $R_t \in \mathbb{R}^{n \times n}$. In particular, the authors of Shampoo (Gupta et al., 2018) proposed to update Kronecker factors using simple formulas based on the current gradient $G_t \in \mathbb{R}^{m \times n}$ of the layer:

$$L_{t+1} = L_t + G_t G_t^\top, \quad R_{t+1} = R_t + G_t^\top G_t. \quad (4)$$

Unfolding these recurrent formulas and starting with $L_0 = \varepsilon I$, $R_0 = \varepsilon I$, (Gupta et al., 2018) aims to substitute the exact empirical Fisher matrix with its theoretically-proven upper bound in the Kronecker product form. Under assumption that every G_i has rank at most r , the authors obtain the following upper bound:

$$\begin{aligned} \varepsilon I_{mn} + \frac{1}{r} F_t &\preceq \\ &\preceq \left(\varepsilon I + \sum_i^t G_i G_i^\top \right)^{\frac{1}{2}} \otimes \left(\varepsilon I + \sum_i^t G_i^\top G_i \right)^{\frac{1}{2}}, \end{aligned}$$

where $A \preceq B$ implies that $B - A$ is a symmetric positive definite matrix. As a result, Shampoo’s preconditioned gradient G'_t can be derived using the following formula:

$$\begin{aligned} \text{vec}(G'_t) &= F_t^{-\frac{1}{2}} \text{vec}(G_t) \approx (L_t^{-\frac{1}{4}} \otimes R_t^{-\frac{1}{4}}) \text{vec}(G_t) = \\ &= \text{vec}(L_t^{-\frac{1}{4}} G_t R_t^{-\frac{1}{4}}). \end{aligned}$$

However, the upper bound defined in Equation 4 may be far from F_t (see Figure 2), and, what is more, taking matrix inverse root of nearly singular matrices

on each optimization step leads to numerical instabilities and is computationally demanding.

SOAP (Vyas et al., 2024) avoids the instability issue by rotating the gradient to align it with the eigenspace of the Fisher matrix and use the diagonal part for preconditioning. The idea behind this approach is that if we are given eigenvalue decompositions of $L_t = Q_L \Lambda_L Q_L^\top$ and $R_t = Q_R \Lambda_R Q_R^\top$, the eigenspace of the Fisher matrix can be approximated using the Kronecker product $Q_L \otimes Q_R$. Indeed, if $\tilde{F}_t \approx L_t \otimes R_t$ then we can rewrite \tilde{F}_t as follows:

$$\begin{aligned} \tilde{F}_t \approx L_t \otimes R_t &= (Q_L \Lambda_L Q_L^\top) \otimes (Q_R \Lambda_R Q_R^\top) = \\ &= (Q_L \otimes Q_R)^\top (\Lambda_L \otimes \Lambda_R) (Q_L \otimes Q_R). \end{aligned}$$

In the eigenbasis of the Kronecker product approximation, the Fisher matrix is expected to be closer to diagonal (we obtain a formal statement in Section 5). As a result, one can replace it with a diagonal matrix in this basis, which is more accurate than for the original matrix without rotations, like in Adam (Kingma and Ba, 2014). Let $\text{vec}(V_t)$ be the diagonal part of the rotated Fisher matrix. Then, we have:

$$\begin{aligned} \text{vec}(G'_t) &= F_t^{-\frac{1}{2}} \text{vec}(G_t) \approx \\ &\approx (Q_L \otimes Q_R) \text{diag}(\text{vec}(V_t))^{-\frac{1}{2}} (Q_L \otimes Q_R)^\top \text{vec}(G_t) = \\ &= (Q_L \otimes Q_R) \text{diag}(\text{vec}(V_t^{\circ-\frac{1}{2}})) \text{vec}(Q_L^\top G_t Q_R) = \\ &= \text{vec}(Q_L ((Q_L^\top G_t Q_R) \oslash V_t^{\circ\frac{1}{2}}) Q_R^\top), \end{aligned}$$

where \oslash denotes elementwise division.

Although (Vyas et al., 2024) introduces a different approach compared to Shampoo, they can be unified from the matrix analysis perspective. Indeed, Shampoo preconditioning can be rewritten as follows:

$$\begin{aligned} \text{vec}(G'_t) &= (L_t^{-\frac{1}{4}} \otimes R_t^{-\frac{1}{4}}) \text{vec}(G_t) \\ &= (Q_L \Lambda_L^{-\frac{1}{4}} Q_L^\top) \otimes (Q_R \Lambda_R^{-\frac{1}{4}} Q_R^\top) \text{vec}(G_t) = \\ &= (Q_L \otimes Q_R) (\Lambda_L \otimes \Lambda_R)^{-\frac{1}{4}} \text{vec}(Q_L^\top G_t Q_R) = \\ &= \text{vec}(Q_L ((Q_L^\top G_t Q_R) \oslash (\Lambda_L \Lambda_R)^{\circ-\frac{1}{4}}) Q_R^\top). \end{aligned}$$

The expression above shows that Shampoo optimizer also rotates the gradient and applies elementwise division in the rotated space, but with an additional constraint for the diagonal.

We argue that maintaining a more accurate approximation of L_t and R_t and, consequently, of Q_L and Q_R may improve the approximation of the Fisher matrix eigenspace in which we rotate the gradient and make the rotated matrix “more diagonal” in terms of the Frobenius norm.

In order to improve the quality of the approximation, we seek to use dynamic low-rank approximation approach, which recently showed its efficiency in full-matrix preconditioning methods in the case of dynamic Cholesky decomposition (Matveeva et al., 2025).

4 Dynamic Low-rank Approximation of the Fisher Information Matrix

Building on the definitions from Section 2 and their properties, in this work we aim to efficiently and accurately maintain the Kronecker product approximation to the empirical Fisher matrix over the optimization steps. Proposition 1 tells us that the approximation of F_t via a Kronecker product can be treated as a rank-1 approximation of the rearranged matrix:

$$\|F_t - L_t \otimes R_t\| = \|\mathcal{R}(F_t) - \text{vec}(L_t) \text{vec}(R_t)^\top\| \rightarrow \min_{L_t, R_t}$$

In (Lubich and Oseledets, 2014; Ceruti et al., 2022), the authors introduce projector-splitting integrators to maintain

an accurate low-rank approximation of the time-dependent matrix trajectory. This approach can also be applied when the matrix undergoes discrete time updates. In Algorithm 1, we adapt the projector-splitting algorithm provided in (Ceruti et al., 2022) for the discrete case. Here and further we will denote a general version of the algorithm as `proj_split`.

Algorithm 1 `proj_split`. Dynamical low-rank approximation with discrete update (Ceruti et al., 2022)

Require: $\tilde{F}_t = U_t S_t V_t^\top$ – current low-rank approximation to F_t ($U \in \mathbb{R}^{m \times r}$, $V \in \mathbb{R}^{n \times r}$ have orthonormal columns, $S \in \mathbb{R}^{r \times r}$ is invertible but not necessary diagonal); $\Delta F_t \in \mathbb{R}^{m \times n}$ – current update of F_t at the step t .

- 1: $\hat{U}_t = U_t S_t + \Delta F_t V_t$;
 - 2: $U_{t+1} S_{t+1} = QR(\hat{U}_t)$;
 - 3: $\hat{V}_t = V_t S_t^\top + \Delta F_t^\top U_t$;
 - 4: $V_{t+1} S_{t+1} = QR(\hat{V}_t)$;
 - 5: $S_{t+1} = U_{t+1}^\top (\tilde{F}_t + \Delta F_t) V_{t+1}$;
 - 6: **return** $\tilde{F}_{t+1} = U_{t+1} S_{t+1} V_{t+1}^\top \approx F_{t+1}$.
-

Note that Algorithm 1 depends only on the current low-rank approximation \tilde{F}_t and the current update ΔF_t . Moreover, the provided algorithm in the case of dynamical rank-1 approximation, which is our case, does not require QR decompositions at all, as they are equivalent to vector normalization.

Now we can adapt Algorithm 1 for our purposes. Here and further we will denote it as `kron_proj_split`. Following the Equation 3, after the rearrangement the update of the Fisher matrix has a particular Kronecker product structure:

$$\mathcal{R}(F_t) = \mathcal{R}(F_{t-1}) + G_t \otimes G_t^\top, \quad (5)$$

implying that $\Delta F_t = G_t \otimes G_t^\top$. Using Equation 1, we observe that the projector-splitting algorithm has an efficient implementation, which does not require matrix-vector products with dense matrices of $mn \times mn$ size. In Algorithm 2, we detail a computationally-efficient implementation of the dynamical low-rank approximation from Algorithm 1 for the matrix F_t defined in Equation 3. A generalization for tensors is presented in Algorithm 5 (Appendix H).

Algorithm 2 `kron_proj_split`. Dynamical Kronecker approximation of Fisher matrix.

Require: $L_t \in \mathbb{R}^{m \times m}$, $R_t \in \mathbb{R}^{n \times n}$ – Kronecker product approximation of the Fisher matrix on the optimization step t , $G_t \in \mathbb{R}^{m \times n}$ – gradient with respect to the layer W_t .

- 1: $\hat{L}_t = L_t \|R_t\|_F + G_t (R_t / \|R_t\|_F) G_t^\top$
 - 2: $\hat{R}_t = R_t \|L_t\|_F + G_t^\top (L_t / \|L_t\|_F) G_t$
 - 3: $L_{t+1} = \hat{L}_t / \|\hat{L}_t\|_F$
 - 4: $R_{t+1} = \hat{R}_t / \|\hat{R}_t\|_F$
 - 5: $S = \langle L_t, L_{t+1} \rangle_F \langle R_t, R_{t+1} \rangle_F + \langle L_{t+1}, G_t R_{t+1} G_t^\top \rangle_F$
 - 6: **return** $S^{1/2} L_{t+1}, S^{1/2} R_{t+1}$
-

This algorithm can be readily inserted in optimizers that rely upon the Kronecker product structure such as SOAP and

Shampoo without noticeable memory and computational overhead. Moreover, we provide a theoretical explanation of the validity of such approach in Proposition 2 which shows that if the Fisher matrix can be accurately approximated with the help of the Kronecker product during training (see (Martens and Grosse, 2015) for motivation), the projector-splitting is able to capture the Kronecker product structure on each step. Let us consider one step of the integrator.

Proposition 2. *Let F_0 and F_1 be such that:*

$$F_0 = A_0 \otimes B_0 + E_0,$$

$$F_1 = A_1 \otimes B_1 + E_1,$$

where $\|E_i\| \leq \varepsilon \|F_i\|$ and $\frac{|\text{tr}((A_0 \otimes B_0)^\top (A_1 \otimes B_1))|}{\|A_0 \otimes B_0\| \|A_1 \otimes B_1\|} \geq c > 0$. Then, one step of the dynamical low-rank approximation from Algorithm 2 starting with $L_0, R_0 = A_0, B_0$ yields the approximation that of F_1 such that:

$$L_1 \otimes R_1 = A_1 \otimes B_1 + \hat{E}_1 + O(\varepsilon^2),$$

where $\|\hat{E}_1\| \leq (1 + \frac{2}{c}) (\|E_1\| + \|E_0\|)$.

Proof. See Appendix B. □

On the contrary, the accuracy of Shampoo approximation depends on the degree of collinearity of the gradients (mutual coherence μ).

Definition 6. *The mutual coherence μ of a set of vectors $\{g_i\}_{i=1}^n$ is defined as:*

$$\mu = \max_{i \neq j} \frac{|g_i^\top g_j|}{\|g_i\| \|g_j\|}.$$

Mutual coherence μ ranges from 0 for pairwise orthogonal vectors (if n is less than size of g_i) to 1 for collinear.

The following proposition shows that the less aligned the vectors $\text{vec}(G_i)$ are, the more is the difference in the norms of Fisher matrix and Shampoo estimate.

Proposition 3. *Let μ_t be the mutual coherence of the gradients $\{\text{vec}(G_i)\}_{i=1}^t$. Let $L_t = \sum_i^t G_i G_i^\top$, $R_t = \sum_i^t G_i^\top G_i$ (as in Shampoo and SOAP). Then*

$$\left\| L_t^{\frac{1}{2}} \otimes R_t^{\frac{1}{2}} \right\|^2 - \|F_t\|^2 \geq (1 - \mu_t^2) \sum_i^t \sum_{j \neq i}^t \|G_i\|^2 \|G_j\|^2.$$

Proof. See Appendix C. □

If the gradients are close to collinear, then $\mu_t \approx 1$ and the norm of Shampoo approximation is close to the true Fisher norm. However, when the directions of the gradients vary, which may occur in practice, the Shampoo approximation becomes less accurate.

To also empirically support our findings, we sample $G_i \in \mathbb{R}^{32 \times 32}$ from $\mathcal{N}(0, I)$ and sum them with exponential moving average $\beta = 0.9$, obtaining the Fisher matrix, following Shampoo optimizer (Gupta et al., 2018) setup. Figure 2

demonstrates the error Fisher matrix approximation with different methods. The error of DyKAF approximation is almost the same as of the best Kronecker product approximation, which means that it is significantly closer to true Fisher matrix, than Shampoo.

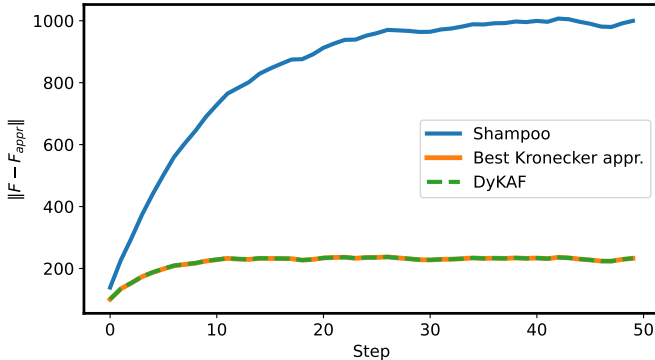


Figure 2: Fisher matrix approximation error with different methods in the case when G_i are sampled from $\mathcal{N}(0, I)$.

5 DyKAF Optimizer

We are now ready to define our modification of the SOAP optimizer, which is the core contribution of our work. DyKAF optimizer (Algorithm 3) incorporates a dynamical Kronecker approximation of the Fisher information matrix using Algorithm 2. Before describing the DyKAF optimizer, let us start with the initialization of Kronecker factors in Algorithm 3.

5.1 Initialization

Unlike Shampoo and SOAP, which initialize Kronecker factors with scaled identity matrices, we start with the best Kronecker approximation of the Fisher matrix on the first step $F_1 = \text{vec}(G_1)\text{vec}(G_1)^\top$. This initialization can be efficiently obtained using the power method for G_1 , as it stated in Proposition 4.

Proposition 4. *The solution to*

$$\min_{L, R} \|\text{vec}(G_1)\text{vec}(G_1)^\top - L \otimes R\|$$

is given by $L = \sigma_1(G_1)u_1u_1^\top$ and $R = \sigma_1(G_1)v_1v_1^\top$, where u_1 and v_1 are the left and the right singular vectors of G_1 corresponding to the largest singular value $\sigma_1(G_1)$.

Proof. See Appendix D. \square

5.2 Adam Second Moment in the Rotated Space

We additionally investigate the estimation of the Fisher matrix eigenvalues. SOAP approximates them using the second moment $V_t \in \mathbb{R}^{m \times n}$ in the rotated space as follows:

$$V_t = \beta_2 V_{t-1} + (1 - \beta_2)(G'_t \odot G'_t).$$

In this work, we introduce an alternative way to estimate eigenvalues of the Fisher matrix.

Let us assume that F has the following form:

$$F_t = L_t \otimes R_t + E_t,$$

where L_t and R_t are the current Kronecker product factors. If we know eigenvalue decompositions $L_t = Q_L \Lambda_L Q_L^\top$ and $R_t = Q_R \Lambda_R Q_R^\top$, then we have

$$\begin{aligned} \tilde{F}_t &= (Q_L \otimes Q_R)^\top F_t (Q_L \otimes Q_R) + E_t \\ &= \Lambda_L \otimes \Lambda_R + \tilde{E}_t, \end{aligned} \quad (6)$$

where $\tilde{E}_t = (Q_L \otimes Q_R)^\top E_t (Q_L \otimes Q_R)$. If we work under assumption that the Fisher matrix can be accurately approximated as a Kronecker product, then \tilde{F}_t is closer to a diagonal matrix than F_t . We provide a more formal version in the following proposition.

Proposition 5. *Let $F \in \mathbb{R}^{mn \times mn}$ be a symmetric matrix which can be represented in the following form:*

$$F_t = A_t \otimes B_t + E_t, \quad (7)$$

where $E_t \in \mathbb{R}^{mn \times mn}$ satisfies $\|E_t\| \leq \|\text{off}(F)\|_{F_t}$, and $A_t \in \mathbb{R}^{m \times m}$, $B_t \in \mathbb{R}^{n \times n}$ are symmetric matrices. Let $A_t = Q_A \Lambda_A Q_A^\top$, $B_t = Q_B \Lambda_B Q_B^\top$ be the eigenvalue decompositions. Then

$$\|\text{diag}((Q_A \otimes Q_B)^\top F_t (Q_A \otimes Q_B))\|_F \geq \|\text{diag}(F_t)\|_F.$$

and

$$\|\text{off}((Q_A \otimes Q_B)^\top F_t (Q_A \otimes Q_B))\|_F \leq \|\text{off}(F_t)\|_F.$$

Proof. See Appendix E. \square

The proposition states that if we have a accurate Kronecker product approximation of the Fisher matrix (Martens and Grosse, 2015), then the rotated matrix \tilde{F}_t is “more diagonal” than F_t in terms of the Frobenius norm. It additionally highlights the importance of having a good approximation of the Q_L and Q_R , as these matrices explicitly affect the proximity of the rotated matrix to the diagonal matrix.

The assumption that the rotated Fisher matrix is close to a diagonal matrix makes it also possible to try a lightweight approximation and efficiently invert it.

At the same time, under the assumptions of Proposition 5 the diagonal part of the rotated matrix \tilde{F}_t can be written in the form

$$\text{diag}(\tilde{F}_t) = \Lambda_L \otimes \Lambda_R + \text{diag}(\tilde{E}_t),$$

which, in the case of small $\|\tilde{E}_t\|$, can be well approximated by Kronecker product of two diagonal matrices. Hence, matrixization of the diagonal of rotated Fisher matrix \tilde{F}_t can be approximated via rank-1 matrix under assumptions in Proposition 5. This allows us to apply the same projector-splitting approach to approximation of the Adam’s second moment, additionally decreasing optimizer’s memory consumption.

5.3 DyKAF Optimizer

Now we are ready to formulate the main algorithm of this work. Algorithm 3 follows the SOAP framework and can be viewed as its modification that uses projector-splitting to keep an accurate dynamical Kronecker approximation, while remaining memory- and time-efficient (see Appendix F.1). It integrates cleanly into existing SOAP code, and, as shown in experiments, working well with the same hyperparameters as SOAP (see Section 6.2).

Regarding the second moment maintenance, DyKAF supports two modes controlled by the flag `rank1_second_moment`. If enabled, the Adam second moment matrix $V_t \in \mathbb{R}^{m \times n}$ is approximated with product of two vectors $v_l \in \mathbb{R}^m$ and $v_r \in \mathbb{R}^n$, which are initialized to small constants $\varepsilon \mathbf{1}$. Otherwise, the standard AdamW is used with initialization $V_0 = 0$. We recommend setting `rank1_second_moment = True` for fine-tuning and `False` for pretraining (see Appendix F.2). The momentum term M_0 is initialized to zero.

Algorithm 3 DyKAF optimizer’s step t for a $m \times n$ layer W_t . *Hyperparameters*: learning rate η , betas (β_1, β_2) , epsilon ε , preconditioning frequency f and Adam rank-1 flag `rank1_second_moment`.

```

1: Sample batch  $B_t$ 
2:  $G_t \in \mathbb{R}^{m \times n} \leftarrow -\nabla_W \mathcal{L}_{B_t}(W_t)$ .
3:  $G'_t \leftarrow Q_L^\top G_t Q_R$ 
4:  $M_t \leftarrow \beta_1 M_t + (1 - \beta_1) G_t$ 
5:  $M'_t \leftarrow Q_L^\top M_t Q_R$ 
6: if rank1_second_moment then
    ▷ Apply alg. 1 to update rank-1 Adam second moment approximation and use in step 10
7:  $v_l v_r^\top \leftarrow \text{proj\_split}(v_l v_r^\top, G'_t \odot M'_t)$ 
8:  $N'_t \leftarrow M'_t \oslash \left( (v_l v_r^\top)^{\circ \frac{1}{2}} + \varepsilon \right)$ 
9: else
10:  $V_t \leftarrow \beta_2 V_t + (1 - \beta_2)(G'_t \odot M'_t)$ 
11:  $N'_t \leftarrow M'_t \oslash \left( V_t^{\circ \frac{1}{2}} + \varepsilon \right)$ 
12:  $N_t \leftarrow Q_L N'_t Q_R^\top$ 
13:  $W_t \leftarrow W_t - \eta N_t$ 
    ▷ Apply alg. 2 to update  $L$  and  $R$ 
14:  $L, R \leftarrow \text{kron\_proj\_split}(\sqrt{\beta_1} L, \sqrt{\beta_1} R, \sqrt{1 - \beta_1} G_t)$ 
15: if  $t \% f = 0$  then
    ▷ Apply alg. 4 to update  $Q_L$  and  $Q_R$ .
16:  $Q_L \leftarrow \text{Eigenvectors}(L, Q_L)$ 
17:  $Q_R \leftarrow \text{Eigenvectors}(R, Q_R)$ 

```

Algorithm 4 Eigenvectors function from (Vyas et al., 2024).

```

1:  $S \leftarrow PQ$ 
2:  $Q \leftarrow \text{QR}(S)$ 

```

6 Experiments

We organize the experimental evaluation into two stages.

First we focus on fine-tuning benchmarks (Section 6.1) and after we move to pretraining tasks (Section 6.2). We compare DyKAF (Algorithm 3) against AdamW (Kingma and Ba, 2014), Muon (Jordan et al., 2024), and SOAP (Vyas et al., 2024). These optimizers constitute a representative set of state-of-the-art methods, combining strong empirical performance with theoretical appeal, and thus form a compelling baseline suite for comparison.

6.1 Fine-tuning

We evaluate DyKAF (Algorithm 3) in two fine-tuning scenarios covering both medium-scale and large-scale models. In all runs, only the self-attention matrices are updated while the rest of the model remains frozen. For DyKAF optimizer we set `rank1_second_moment` parameter to `True`, which is motivated by the empirical observation that the gradients in fine-tuning exhibit low-rank structure (see ablation study in Appendix F.2). Other hyperparameter details are provided in Appendix G.1.

Sentence-level language understanding. Our first setup considers `Roberta-Large` model (He et al., 2021) (185M parameters) on the GLUE benchmark (Wang et al., 2018). We adopt full fine-tuning of the self-attention matrices, i.e., without any parameter-efficient adapters. This represents a controlled medium-scale setting where optimization dynamics can be clearly compared. The results are reported in Table 1.

Table 1: Results on the GLUE benchmark with full fine-tuning of `Roberta-Large` (185M). Only the self-attention matrices are updated, while all other parameters remain frozen. The best result per column is shown in bold and the second-best is underlined.

Method	MNLI	SST-2	CoLA	QQP	QNLI	RTE	MRPC	ALL
	Acc	Acc	Mcc	Acc	Acc	Acc	Acc	Avg
AdamW	90.13	95.87	<u>68.66</u>	92.24	94.00	<u>83.03</u>	<u>89.95</u>	<u>87.70</u>
Muon	89.94	<u>95.18</u>	68.73	91.88	93.32	80.51	<u>89.95</u>	87.07
SOAP	<u>90.03</u>	94.84	67.53	91.86	93.30	81.23	88.73	86.79
DyKAF	90.01	96.45	68.44	<u>92.16</u>	<u>93.54</u>	84.48	90.93	88.00

LLM downstream adaptation. To test transferability in large-scale settings, we further evaluate `Qwen3-8B` model (Yang et al., 2025) across classical LLM benchmarks: MathQA (Yu et al., 2023), GSM8K (Cobbe et al., 2021), HellaSwag (Zellers et al., 2019), BoolQ (Clark et al., 2019) and ARC-Challenge (Clark et al., 2018). Unlike the GLUE case, here we employ LoRA adapters (Hu et al., 2021) for practical efficiency, reflecting a more realistic adaptation pipeline for modern LLMs. This benchmark emphasizes sample efficiency and robustness to heterogeneous reasoning and comprehension tasks. The corresponding results are presented in Table 2.

Fine-tuning experiment results. Across both setups DyKAF achieves the strongest overall performance. On the GLUE benchmark with full fine-tuning of `Roberta-Large`, DyKAF attains the highest average score, consistently

Table 2: Results on LLM fine-tuning with Qwen3-8B using LoRA on self-attention matrices. We evaluate different optimizers across classical LLM benchmarks. The best result per column is shown in bold and the second-best is underlined.

Method	MathQA Acc	GSM8K Acc	HellaSwag Acc	BoolQ Acc	ARC Acc	ALL Avg
AdamW	<u>43</u>	<u>40</u>	<u>69</u>	63	85	60.0
Muon	<u>43</u>	42	<u>69</u>	<u>64</u>	85	<u>60.6</u>
SOAP	41	42	68	63	89	<u>60.6</u>
DyKAF	47	39	70	67	<u>86</u>	61.8

matching or surpassing baselines on most tasks. On the large-scale LLM experiments with Qwen3-8B, DyKAF again achieves the best average result, with particularly strong gains on reasoning-oriented datasets such as MathQA and BoolQ. These findings demonstrate that DyKAF provides competitive advantages in both medium-scale and large-scale fine-tuning regimes, outperforming widely used optimizers including AdamW, Muon, and SOAP.

6.2 Pretraining

We evaluate DyKAF (Algorithm 3) in two pretraining scenarios, spanning small- to medium-scale (NanoGPT-like) and larger-scale (LLaMA-124M on FineWeb). In all fine-tuning experiments with DyKAF optimizer we set `rank1_second_moment = False` in Algorithm 3, supported by an ablation study (Appendix F.2), which shows that, unlike in fine-tuning, pretraining benefits from retaining a full-rank second-moment estimate. Other hyperparameter details are provided in Appendix G.2.

Character-level language modeling. We first evaluate small-scale GPT-base model using Shakespeare-char dataset (~ 160 M tokens) (Caldas et al., 2018) following the NanoGPT setup (Karpathy, 2022). We consider models of varying sizes (0.41M, 1.55M, 3.24M parameters) and report minimum validation loss for each scale. Results are presented in Table 3.

Table 3: Pretraining on Shakespeare-char with GPT-base models of varying sizes. We report minimum validation loss for different model sizes. The best result per column is shown in bold and the second-best is underlined.

Method	0.41M min val loss	1.55M min val loss	3.24M min val loss	ALL Avg
AdamW	<u>1.5923</u>	1.5893	1.5614	1.5810
Muon	1.6430	1.6218	1.6160	1.6269
SOAP	1.5954	<u>1.5749</u>	<u>1.5474</u>	<u>1.5726</u>
DyKAF	1.5797	1.5671	1.5346	1.5605

Large-scale web corpus pretraining. We next follow the large-scale setup introduced in (Semenov et al., 2025b), pretraining LLaMA-124M (Dubey et al., 2024) on the FineWeb dataset (~ 100 B tokens) (Penedo et al., 2024).

In all previous experiments, competing optimizers were re-implemented and tuned under identical conditions. For this large-scale setting, however, we directly adopted the reported results of AdamW, Muon, and SOAP from (Semenov et al., 2025b). DyKAF was run with the same hyperparameters as SOAP in that benchmark, since pretraining runs at this scale are prohibitively expensive, making a dedicated hyperparameter sweep infeasible. Results are deferred to Table 4.

Table 4: Pretraining on FineWeb with LLaMA-124M. Reported values are validation losses after different number of processed training tokens. The best result per column is shown in bold and the second-best is underlined.

Method	1B val loss	2.1B val loss	4.2B val loss	6.3B val loss	8.4B val loss	16.8B val loss	ALL Avg
AdamW	3.5098	3.3992	3.3128	3.2752	3.2522	<u>3.2083</u>	3.3263
Muon	<u>3.4626</u>	<u>3.3662</u>	<u>3.2953</u>	<u>3.2639</u>	3.2445	3.2111	3.3073
SOAP	3.4731	3.3735	3.3006	<u>3.2637</u>	<u>3.2437</u>	3.2149	3.3116
DyKAF	3.4553	3.3568	3.2832	3.2464	3.2319	3.1986	3.2954

Pretraining experiment results. Pretraining experiments require substantially larger computational resources than fine-tuning, with models trained on billions of tokens and long wall-clock times. Across all settings DyKAF achieves the strongest results, outperforming baseline optimizers. On the small-scale GPT-base pretraining, DyKAF consistently obtains the lowest validation loss across model sizes. In the large-scale LLaMA-124M pretraining, DyKAF again surpasses the baselines. Importantly, in this most resource-intensive experiment we reuse the SOAP hyperparameters without any additional tuning, nevertheless DyKAF remains robust and yields state-of-the-art results, highlighting the stability of the method under challenging large-scale training conditions.

7 Related Work

K-FAC approximates the layerwise Fisher with a Kronecker product, lowering cost while preserving key curvature (Martens and Grosse, 2015). Extensions to convolutional layers exploit spatial sharing for practical speedups (Grosse and Martens, 2016; Tornstad, 2020). Empirically, K-FAC-style preconditioners offer a strong accuracy-efficiency trade-off, motivating low-rank and block variants (Ren et al., 2021; Koroko et al., 2023).

Shampoo builds on K-FAC by preconditioning with matrix powers, using the $-1/4$ exponent to shape gradient updates and improve convergence stability (Gupta et al., 2018). A distributed, numerically robust implementation (Shi et al., 2023) achieves state-of-the-art results and wins AlgoPerf (Dahl et al., 2023; Kasimbeg et al., 2025). Recent theory shows that the square of Shampoo’s approximation equals one step of a power method toward the optimal Kronecker-factored Fisher, clarifying its performance (Morwani et al., 2024).

SOAP builds on Shampoo by applying an AdamW-like step

in a Shampoo-preconditioned parameter space and replacing costly matrix roots with fast QR decompositions (Vyas et al., 2024). In large-scale experiments, SOAP shows faster convergence than AdamW and Shampoo across standard benchmarks, supporting its use as a strong default in practice (Semenov et al., 2025b; Wen et al., 2025).

Recent work proposes targeted modifications to the Kronecker-based preconditioners used in SOAP and Shampoo, aiming to stabilize curvature and keep costs modest. Fisher-Orthogonal Projection adds structured projections to stabilize Fisher estimates in large models (Lu and Armour, 2025). Two algorithms refine the Fisher approximation with block structure and low rank while maintaining Kronecker-like update cost (Gong et al., 2025). KL-aligned preconditioners further improve the performance of second-order steps (Lin et al., 2025). Overall, these studies sharpen Kronecker-based approximations with simple mechanisms and practical overheads.

8 Conclusion

This paper proposes a dynamical Kronecker approximation of the empirical Fisher matrix within a SOAP-style preconditioner, maintained via a projector-splitting algorithm, enabling stable curvature-aware training with minimal overhead while preserving layerwise structure. Experiments on language understanding, LLM adaptation, and pretraining show improved performance over strong baselines without extensive hyperparameter sweeps.

References

Akiba, T., Sano, S., Yanase, T., Ohta, T., and Koyama, M. (2019). Optuna: A next-generation hyperparameter optimization framework. In *Proceedings of the 25th ACM SIGKDD international conference on knowledge discovery & data mining*, pages 2623–2631.

Amari, S.-I. (1998). Natural gradient works efficiently in learning. *Neural computation*, 10(2):251–276.

Caldas, S., Duddu, S. M. K., Wu, P., Li, T., Konečný, J., McMahan, H. B., Smith, V., and Talwalkar, A. (2018). Leaf: A benchmark for federated settings. *arXiv preprint arXiv:1812.01097*.

Ceruti, G., Kusch, J., and Lubich, C. (2022). A rank-adaptive robust integrator for dynamical low-rank approximation. *BIT Numerical Mathematics*, 62(4):1149–1174.

Chang, C.-C. and Lin, C.-J. (2011). Libsvm: A library for support vector machines. *ACM transactions on intelligent systems and technology (TIST)*, 2(3):1–27.

Clark, C., Lee, K., Chang, M.-W., Kwiatkowski, T., Collins, M., and Toutanova, K. (2019). Boolq: Exploring the surprising difficulty of natural yes/no questions. *arXiv preprint arXiv:1905.10044*.

Clark, P., Cowhey, I., Etzioni, O., Khot, T., Sabharwal, A., Schoenick, C., and Tafjord, O. (2018). Think you have solved question answering? try arc, the ai2 reasoning challenge. *arXiv preprint arXiv:1803.05457*.

Cobbe, K., Kosaraju, V., Bavarian, M., Chen, M., Jun, H., Kaiser, L., Plappert, M., Tworek, J., Hilton, J., Nakano, R., et al. (2021). Training verifiers to solve math word problems. *arXiv preprint arXiv:2110.14168*.

Dahl, G. E., Schneider, F., Nado, Z., Agarwal, N., Sastry, C. S., Hennig, P., Medapati, S., Eschenhagen, R., Kasimbeg, P., Suo, D., Bae, J., Gilmer, J., Peirson, A. L., Khan, B., Anil, R., Rabbat, M., Krishnan, S., Snider, D., Amid, E., Chen, K., Maddison, C. J., Vasudev, R., Badura, M., Garg, A., and Mattson, P. (2023). Benchmarking Neural Network Training Algorithms.

Dubey, A., Jauhri, A., Pandey, A., Kadian, A., Al-Dahle, A., Letman, A., Mathur, A., Schelten, A., Yang, A., Fan, A., et al. (2024). The Llama 3 herd of models. *arXiv preprint arXiv:2407.21783*.

Frantar, E., Kurtic, E., and Alistarh, D. (2021). M-fac: Efficient matrix-free approximations of second-order information. *Advances in Neural Information Processing Systems*, 34:14873–14886.

Golub, G. H. and Van Loan, C. F. (2013). *Matrix computations*. JHU press.

Gong, W., Scetbon, M., Ma, C., and Meeds, E. (2025). Towards efficient optimizer design for llm via structured fisher approximation with a low-rank extension. *arXiv preprint arXiv:2502.07752*.

Goodfellow, I., Bengio, Y., Courville, A., and Bengio, Y. (2016). *Deep learning*, volume 1. MIT press Cambridge.

Grosse, R. and Martens, J. (2016). A kronecker-factored approximate fisher matrix for convolution layers. In *International Conference on Machine Learning*, pages 573–582. PMLR.

Gupta, V., Koren, T., and Singer, Y. (2018). Shampoo: Preconditioned stochastic tensor optimization. In *International Conference on Machine Learning*, pages 1842–1850. PMLR.

He, P., Gao, J., and Chen, W. (2021). Debertav3: Improving deberta using electra-style pre-training with gradient-disentangled embedding sharing. *arXiv preprint arXiv:2111.09543*.

Hernández-Cano, A., Hägele, A., Huang, A. H., Romanou, A., Solergibert, A.-J., Pasztor, B., Messmer, B., Garbaya, D., Durech, E. F., Hakimi, I., et al. (2025). Apertus: Democratizing open and compliant llms for global language environments. *arXiv preprint arXiv:2509.14233*.

Hu, E. J., Shen, Y., Wallis, P., Allen-Zhu, Z., Li, Y., Wang, S., Wang, L., and Chen, W. (2021). LoRA: Low-rank adaptation of large language models. *arXiv preprint arXiv:2106.09685*.

Jordan, K., Jin, Y., Boza, V., Jiacheng, Y., Cecista, F., Newhouse, L., and Bernstein, J. (2024). Muon: An optimizer for hidden layers in neural networks.

Karpathy, A. (2022). NanoGPT. <https://github.com/karpathy/nanoGPT>.

Kasimbeg, P., Schneider, F., Eschenhagen, R., Bae, J., Sastry, C. S., Saroufim, M., Boyuan, F., Wright, L., Yang,

- E. Z., Nado, Z., Medapati, S., Hennig, P., Rabbat, M., and Dahl, G. E. (2025). Accelerating neural network training: An analysis of the AlgoPerf competition. In *The Thirteenth International Conference on Learning Representations*.
- Kingma, D. P. and Ba, J. (2014). Adam: A method for stochastic optimization. *arXiv preprint arXiv:1412.6980*.
- Koroko, A., Anciaux-Sedrakian, A., Gharbia, I. B., Garès, V., Haddou, M., and Tran, Q. H. (2023). Efficient approximations of the fisher matrix in neural networks using kronecker product singular value decomposition. *ESAIM: Proceedings and Surveys*, 73:218–237.
- Kunstner, F., Hennig, P., and Balles, L. (2019). Limitations of the empirical fisher approximation for natural gradient descent. *Advances in neural information processing systems*, 32.
- Lin, W., Lowe, S. C., Dangel, F., Eschenhagen, R., Xu, Z., and Grosse, R. B. (2025). Understanding and improving the shampoo optimizer via kullback-leibler minimization. *arXiv preprint arXiv:2509.03378*.
- Lu, Y. and Armour, W. (2025). Fisher-orthogonal projection methods for natural gradient descent with large batches. *arXiv preprint arXiv:2508.13898*.
- Lubich, C. and Oseledets, I. V. (2014). A projector-splitting integrator for dynamical low-rank approximation. *BIT Numerical Mathematics*, 54(1):171–188.
- Martens, J. (2020). New insights and perspectives on the natural gradient method. *Journal of Machine Learning Research*, 21(146):1–76.
- Martens, J. and Grosse, R. (2015). Optimizing neural networks with kronecker-factored approximate curvature. In *International conference on machine learning*, pages 2408–2417. PMLR.
- Matveeva, T., Katrutsa, A., and Frolov, E. (2025). Dynamic low-rank approximation of full-matrix preconditioner for training generalized linear models. *arXiv preprint arXiv:2508.21106*.
- Morwani, D., Shapira, I., Vyas, N., Malach, E., Kakade, S., and Janson, L. (2024). A new perspective on shampoo’s preconditioner. *arXiv preprint arXiv:2406.17748*.
- Parthasarathy, V. B., Zafar, A., Khan, A., and Shahid, A. (2024). The ultimate guide to fine-tuning llms from basics to breakthroughs: An exhaustive review of technologies, research, best practices, applied research challenges and opportunities. *arXiv preprint arXiv:2408.13296*.
- Penedo, G., Kydlíček, H., Lozhkov, A., Mitchell, M., Raffel, C. A., Von Werra, L., Wolf, T., et al. (2024). The fineweb datasets: Decanting the web for the finest text data at scale. *Advances in Neural Information Processing Systems*, 37:30811–30849.
- Ren, Y., Bahamou, A., and Goldfarb, D. (2021). Kronecker-factored quasi-newton methods for deep learning. *arXiv preprint arXiv:2102.06737*.
- Rumelhart, D., Hinton, G., and Williams, R. (1986). Learning representations by back-propagating errors. *Nature*, 323(6088):533–536.
- Semenov, A., Jaggi, M., and Doikov, N. (2025a). Gradient-normalized smoothness for optimization with approximate hessians. *arXiv preprint arXiv:2506.13710*.
- Semenov, A., Pagliardini, M., and Jaggi, M. (2025b). Benchmarking optimizers for large language model pretraining. *arXiv preprint arXiv:2509.01440*.
- Shi, H.-J. M., Lee, T.-H., Iwasaki, S., Gallego-Posada, J., Li, Z., Rangadurai, K., Mudigere, D., and Rabbat, M. (2023). A distributed data-parallel pytorch implementation of the distributed shampoo optimizer for training neural networks at-scale. *arXiv preprint arXiv:2309.06497*.
- Team, K., Bai, Y., Bao, Y., Chen, G., Chen, J., Chen, N., Chen, R., Chen, Y., Chen, Y., Chen, Y., et al. (2025). Kimi k2: Open agentic intelligence. *arXiv preprint arXiv:2507.20534*.
- Tornstad, M. (2020). Evaluating the practicality of using a kronecker-factored approximate curvature matrix in newton’s method for optimization in neural networks.
- Veprikov, A., Solodkin, V., Zyl, A., Savchenko, A., and Beznosikov, A. (2025). Weightlora: Keep only necessary adapters. *arXiv preprint arXiv:2506.02724*.
- Vyas, N., Morwani, D., Zhao, R., Kwun, M., Shapira, I., Brandfonbrener, D., Janson, L., and Kakade, S. (2024). Soap: Improving and stabilizing shampoo using adam. *arXiv preprint arXiv:2409.11321*.
- Wang, A., Singh, A., Michael, J., Hill, F., Levy, O., and Bowman, S. R. (2018). Glue: A multi-task benchmark and analysis platform for natural language understanding. *arXiv preprint arXiv:1804.07461*.
- Wen, K., Hall, D., Ma, T., and Liang, P. (2025). Fantastic pretraining optimizers and where to find them. *arXiv preprint arXiv:2509.02046*.
- Wu, X., Yu, W., Zhang, C., and Woodland, P. (2024). An improved empirical fisher approximation for natural gradient descent. *Advances in Neural Information Processing Systems*, 37:134151–134194.
- Yang, A., Li, A., Yang, B., Zhang, B., Hui, B., Zheng, B., Yu, B., Gao, C., Huang, C., Lv, C., et al. (2025). Qwen3 technical report. *arXiv preprint arXiv:2505.09388*.
- Yu, L., Jiang, W., Shi, H., Yu, J., Liu, Z., Zhang, Y., Kwok, J. T., Li, Z., Weller, A., and Liu, W. (2023). Metamath: Bootstrap your own mathematical questions for large language models. *arXiv preprint arXiv:2309.12284*.
- Zellers, R., Holtzman, A., Bisk, Y., Farhadi, A., and Choi, Y. (2019). Hellaswag: Can a machine really finish your sentence? *arXiv preprint arXiv:1905.07830*.

Supplementary Materials

A Empirical Studies on Hessian Accuracy

A.1 Hessian of the Softmax Cross-Entropy Loss

Setup. For a single training pair (x, y) with $x \in \mathbb{R}^n$ and one-hot $y \in \{e_1, \dots, e_m\}$, let

$$z = Wx, \quad p = \text{softmax}(z), \quad p_k = \frac{\exp(z_k)}{\sum_{j=1}^m \exp(z_j)},$$

where $W \in \mathbb{R}^{m \times n}$ and $z, p \in \mathbb{R}^m$. The per-sample cross-entropy loss is

$$L(W) = -\sum_{k=1}^m y_k \log p_k.$$

Gradient. The softmax Jacobian is

$$\frac{\partial p_i}{\partial z_j} = p_i(\delta_{ij} - p_j).$$

Using it together with $\partial(-\log p_k)/\partial p_k = -1/p_k$,

$$\frac{\partial L}{\partial z_j} = \sum_{k=1}^m \left(-\frac{y_k}{p_k}\right) p_k(\delta_{kj} - p_j) = p_j - y_j \implies \nabla_z L = p - y.$$

Because $z = Wx$ and $\partial z_j / \partial W_{jk} = x_k$,

$$\nabla_W L = (p - y) x^\top \in \mathbb{R}^{m \times n}.$$

Hessian. Start from the element-wise gradient

$$\frac{\partial L}{\partial W_{ij}} = (p_i - y_i) x_j, \quad i = 1, \dots, m, \quad j = 1, \dots, n,$$

and differentiate once more with respect to another entry W_{kl} :

$$\frac{\partial^2 L}{\partial W_{ij} \partial W_{kl}} = x_j \frac{\partial(p_i - y_i)}{\partial W_{kl}} = x_j \frac{\partial p_i}{\partial W_{kl}}.$$

Because $z = Wx$, the logit derivatives are

$$\frac{\partial z_r}{\partial W_{kl}} = x_l \delta_{rk}.$$

Using the soft-max Jacobian $\frac{\partial p_i}{\partial z_r} = p_i(\delta_{ir} - p_r)$,

$$\frac{\partial p_i}{\partial W_{kl}} = \sum_{r=1}^m \frac{\partial p_i}{\partial z_r} \frac{\partial z_r}{\partial W_{kl}} = p_i(\delta_{ik} - p_k) x_l.$$

Substituting,

$$\frac{\partial^2 L}{\partial W_{ij} \partial W_{kl}} = p_i(\delta_{ik} - p_k) x_j x_l \quad (i, j, k, l).$$

Let $H^{(z)} = \text{diag}(p) - pp^\top \in \mathbb{R}^{m \times m}$ and $S = xx^\top \in \mathbb{R}^{n \times n}$. Vectorising W into $w = \text{vec}(W) \in \mathbb{R}^{mn}$, the Hessian becomes

$$\nabla_W^2 L = H^{(z)} \otimes S \in \mathbb{R}^{(mn) \times (mn)},$$

i.e. a Kronecker product of the *predictive covariance* $H^{(z)}$ and the *input covariance* S .

Dataset loss. For a dataset $\{(x_i, y_i)\}_{i=1}^N$ define the empirical loss

$$L(W) = -\frac{1}{N} \sum_{i=1}^N \sum_{k=1}^m y_{ik} \log p_{ik}, \quad p_i = \text{softmax}(Wx_i).$$

Its first and second derivatives are the averages

$$\nabla_W L = \frac{1}{N} \sum_{i=1}^N (p_i - y_i) x_i^\top, \quad \nabla_W^2 L = \frac{1}{N} \sum_{i=1}^N \left(\text{diag}(p_i) - p_i p_i^\top \right) \otimes (x_i x_i^\top).$$

Hence the full-batch Hessian remains a sum of Kronecker products of input covariances $x_i x_i^\top$ and predictive covariances $\text{diag}(p_i) - p_i p_i^\top$.

A.2 Experiment Details

We examine the accuracy of Hessian approximation on a controlled setup: multiclass classification of the `mushrooms` dataset (Chang and Lin, 2011) with an MLP and softmax output. In this case the exact Hessian can be computed analytically (see Appendix A.1), enabling a direct comparison of the Fisher matrix estimates from SOAP and DyKAF with real Hessian matrix. We evaluate the difference for varying numbers of available training samples, with optimizer hyperparameters tuned via Optuna package (Akiba et al., 2019). For both SOAP and DyKAF, we build the full Fisher matrix approximation using the following formula:

$$\tilde{F}_{\text{method}} = (Q_L \otimes Q_R) \text{diag}(\text{vec}(V_t)) (Q_L \otimes Q_R)^\top,$$

where Q_L, Q_R and V_t are taken from Algorithm 3. Motivated by (Martens and Grosse, 2015), we use $\tilde{F}_{\text{method}}$ as Hessian approximation and report the Frobenius norm of the difference between the real Hessian and its estimates $\|H_{\text{real}} - \tilde{F}_{\text{method}}\|$. Figure 1 shows that DyKAF consistently yields a more accurate Hessian approximation than SOAP across various settings.

B Proof of Proposition 2

Proof. Let for the sake of brevity $\tilde{A} = \mathcal{R}(A)$ in this section. Applying rearrangement operator to F_0 and F_1 , we obtain

$$\begin{aligned} \tilde{F}_0 &= \mathcal{R}(F_0) = \mathcal{R}(L_0 \otimes R_0 + E_0) = s_0 \ell_0 r_0^\top + \tilde{E}_0, \\ \tilde{F}_1 &= \mathcal{R}(F_1) = \mathcal{R}(F_0 + \Delta F) = \mathcal{R}(A_1 \otimes B_1 + E_1) = sab^\top + \tilde{E}_1, \end{aligned}$$

where $\Delta F = F_1 - F_0$; the vectors $\ell_0 = \text{vec}(L_0)/\|L_0\|, r_0 = \text{vec}(R_0)/\|R_0\|, a = \text{vec}(A_1)/\|A_1\|, b = \text{vec}(B_1)/\|B_1\|$ have norm 1; the values $s_0 = \|A_0 \otimes B_0\| = \|L_0 \otimes R_0\|, s = \|A_1 \otimes B_1\|$ are positive scalars. Let us denote $\tilde{E} = \tilde{E}_1 - \tilde{E}_0$.

We want to apply projector-splitting to approximate $\mathcal{R}(F_1) = \mathcal{R}(F_0) + \mathcal{R}(\Delta F)$, where the current rank-1 approximation to $\mathcal{R}(F_0)$ is $s_0 \ell_0 r_0^\top$. The target dynamical low-rank approximation to \tilde{F}_1 is $\ell_1 s_1 r_1^\top$, where $s_1 = \ell_1^\top (s_0 \ell_0 r_0^\top + \mathcal{R}(\Delta F)) r_1 = \ell_1^\top (\tilde{F}_1 - \tilde{E}_0) r_1$ by formula from Algorithm 1. Now we aim to sequentially obtain the necessary formula, separately deriving all the projector-splitting components.

Using Algorithm 1, we obtain:

$$\ell_1 = \frac{\ell_0 s_0 + \mathcal{R}(\Delta F) r_0}{\|\ell_0 s_0 + \mathcal{R}(\Delta F) r_0\|} = \frac{(\ell_0 r_0^\top s_0 + \mathcal{R}(\Delta F)) r_0}{\|(\ell_0 r_0^\top s_0 + \mathcal{R}(\Delta F)) r_0\|} = \frac{(\tilde{F}_1 - \tilde{E}_0) r_0}{\|(\tilde{F}_1 - \tilde{E}_0) r_0\|} = \frac{(sab^\top + \tilde{E}) r_0}{\|(sab^\top + \tilde{E}) r_0\|}.$$

Let us denote $x = r_0^\top b$ and $y = r_0^\top \tilde{E}^\top a$.

$$d = \|(sab^\top + \tilde{E}) r_0\|^2 = r_0^\top (sba^\top + \tilde{E}^\top) (sab^\top + \tilde{E}) r_0 = s^2 (r_0^\top b)^2 + 2s (r_0^\top b) (r_0^\top \tilde{E}^\top a) + O(\varepsilon^2) = s^2 x^2 + 2sxy + O(\varepsilon^2).$$

$$d^{-1} = \frac{1}{s^2 x^2} (1 - 2 \frac{y}{sx} + O(\varepsilon^2)) = \frac{1}{s^2 x^2} - 2 \frac{y}{s^3 x^3} + O(\varepsilon^2).$$

Let us substitute the this expression into the formula for $\ell_1 \ell_1^\top (\tilde{F}_1 - \tilde{E}_0)$:

$$\begin{aligned} \ell_1 \ell_1^\top (\tilde{F}_1 - \tilde{E}_0) &= \frac{(ab^\top s + \tilde{E}) r_0 r_0^\top (ba^\top s + \tilde{E}^\top) (ab^\top s + \tilde{E})}{\|(ab^\top s + \tilde{E}) r_0\|^2} = \\ &= \left(ab^\top s^3 (b^\top r_0)^2 + s^2 (r_0^\top b) (\tilde{E} r_0 b^\top) + s^2 (b^\top r_0) (a r_0^\top \tilde{E}^\top a b^\top) + s^2 (r_0 b^\top)^2 (a a^\top \tilde{E}) + O(\varepsilon^2) \right) d^{-1} = \\ &= \left(ab^\top s^3 x^2 + s^2 x (\tilde{E} r_0 b^\top) + s^2 x (a r_0^\top \tilde{E}^\top a b^\top) + s^2 x^2 (a a^\top \tilde{E}) + O(\varepsilon^2) \right) \left(\frac{1}{s^2 x^2} - 2 \frac{(r_0^\top \tilde{E}^\top a)}{s^3 x^3} + O(\varepsilon^2) \right) = \\ &= ab^\top s - \frac{2ab^\top y}{x} + \frac{\tilde{E} r_0 b^\top}{x} + \frac{ab^\top y}{x} + a a^\top \tilde{E} + O(\varepsilon^2) \end{aligned}$$

The same way,

$$r_1 = \frac{(sab^\top + \tilde{E})^\top \ell_0}{\|(sab^\top + \tilde{E})^\top \ell_0\|}.$$

Let us denote $z = \ell_0^\top a$ and $p = b^\top \tilde{E}^\top \ell_0$.

$$\|(sab^\top + \tilde{E})^\top \ell_0\|^{-2} = \frac{1}{s^2 z^2} - 2 \frac{p}{s^3 z^3} + O(\varepsilon^2).$$

Now, we are able to rewrite $r_1 r_1^\top$ and fully assemble $s_1 l_1 r_1^\top$.

$$\begin{aligned} r_1 r_1^\top &= \left((sba^\top + \tilde{E}^\top) \ell_0 \ell_0^\top (sab^\top + \tilde{E}) \right) \left(\frac{1}{s^2 z^2} - 2 \frac{p}{s^3 z^3} + O(\varepsilon^2) \right) = \\ &= \left(s^2 z^2 bb^\top + sz b \ell_0^\top \tilde{E} + sz \tilde{E}^\top \ell_0 b^\top + O(\varepsilon^2) \right) \left(\frac{1}{s^2 z^2} - 2 \frac{p}{s^3 z^3} + O(\varepsilon^2) \right) = \\ &= bb^\top - 2 \frac{pbb^\top}{sz} + \frac{b \ell_0^\top \tilde{E}}{sz} + \frac{E^\top \ell_0 b^\top}{sz} + O(\varepsilon^2) \end{aligned}$$

Finally, we estimate $\ell_1 s_1 r_1^\top$:

$$\begin{aligned} \ell_1 s_1 r_1^\top &= \ell_1 \ell_1^\top (\tilde{F}_1 - \tilde{E}_0) r_1 r_1^\top = \\ &= \left(ab^\top s - \frac{2ab^\top y}{x} + \frac{\tilde{E} r_0 b^\top}{x} + \frac{ab^\top y}{x} + aa^\top \tilde{E} + O(\varepsilon^2) \right) \left(bb^\top - 2 \frac{pbb^\top}{sz} + \frac{b \ell_0^\top \tilde{E}}{sz} + \frac{E^\top \ell_0 b^\top}{sz} + O(\varepsilon^2) \right) = \\ &= ab^\top s - \frac{2pab^\top}{z} + \frac{a \ell_0^\top \tilde{E}}{z} + \frac{pab^\top}{z} - \frac{2yab^\top}{x} + \frac{\tilde{E} r_0 b^\top}{x} + \frac{yab^\top}{x} + aa^\top \tilde{E} bb^\top + O(\varepsilon^2) = \\ &= ab^\top s + \frac{1}{\ell_0^\top a} \left(-(b^\top \tilde{E}^\top \ell_0) ab^\top + a \ell_0^\top \tilde{E} \right) + \frac{1}{r_0^\top b} \left(-(r_0^\top \tilde{E}^\top a) ab^\top + \tilde{E} r_0 b^\top \right) + aa^\top \tilde{E} bb^\top + O(\varepsilon^2) = \\ &= ab^\top + \hat{E}_1 + O(\varepsilon^2). \end{aligned}$$

Let us estimate the norms of the summands constituting \tilde{E}_1 , which contain the first-order error \tilde{E} .

$$\|aa^\top \tilde{E} bb^\top\| \leq \|aa^\top\| \|\tilde{E}\| \|bb^\top\| = \|\tilde{E}\|.$$

For any matrices C and D of correct sizes, $\|CD\|_F \leq \|C\|_F \|D\|_2$, where $\|\cdot\|_F$ is Frobenius norm (which we have always denoted as $\|\cdot\|$) and $\|\cdot\|_2$ is the spectral norm. The spectral norm of orthoprojector equals 1: $\|I - bb^\top\|_2 = 1$. Therefore,

$$\left\| \frac{1}{\ell_0^\top a} \left(-(b^\top \tilde{E}^\top \ell_0) ab^\top + a \ell_0^\top \tilde{E} \right) \right\|_F = \frac{\|a \ell_0^\top \tilde{E} (I - bb^\top)\|_F}{|\ell_0^\top a|} \leq \frac{\|a \ell_0^\top\|_F \|\tilde{E}\|_F \|I - bb^\top\|_2}{|\ell_0^\top a|} = \frac{\|\tilde{E}\|_F}{|\ell_0^\top a|}.$$

Analogously,

$$\left\| \frac{1}{r_0^\top b} \left(-(r_0^\top \tilde{E}^\top a) ab^\top + \tilde{E} r_0 b^\top \right) \right\| \leq \frac{\|\tilde{E}\|}{|r_0^\top b|}.$$

Therefore,

$$\ell_1 s_1 r_1^\top = ab^\top s + \hat{E}_1 + O(\varepsilon^2),$$

where $\|\hat{E}_1\| \leq \left(1 + \frac{1}{|\ell_0^\top a|} + \frac{1}{|r_0^\top b|} \right) \|\tilde{E}\|$.

Let us remember that

$$|\ell_0^\top a| = \frac{|\text{tr}(A_0^\top A_1)|}{\|A_0\| \|A_1\|}$$

and

$$|r_0^\top b| = \frac{|\text{tr}(B_0^\top B_1)|}{\|B_0\| \|B_1\|}.$$

We know from Cauchy-Schwarz inequality that

$$\frac{|\text{tr}(A_0^\top A_1)|}{\|A_0\| \|A_1\|} \leq 1.$$

Using the condition from the proposition, we get

$$\frac{|\text{tr}((A_0 \otimes B_0)^\top (A_1 \otimes B_1))|}{\|A_0 \otimes B_0\| \|A_1 \otimes B_1\|} \geq c > 0 \quad \Rightarrow \quad \frac{|\text{tr}(B_0^\top B_1)|}{\|B_0\| \|B_1\|} \geq \frac{|\text{tr}(A_0^\top A_1)| |\text{tr}(B_0^\top B_1)|}{\|A_0\| \|A_1\| \|B_0\| \|B_1\|} \geq c.$$

Analogously,

$$|\ell_0^T a| = \frac{|\text{tr}(A_0^\top A_1)|}{\|A_0\| \|A_1\|} \geq c.$$

Therefore,

$$\|\hat{E}_1\| \leq \left(1 + \frac{1}{|\ell_0^T a|} + \frac{1}{|r_0^T b|}\right) \|\tilde{E}\| = \left(1 + \frac{1}{|\ell_0^T a|} + \frac{1}{|r_0^T b|}\right) \|E\| \leq \left(1 + \frac{2}{c}\right) \|E\| \leq \left(1 + \frac{2}{c}\right) (\|E_1\| + \|E_0\|).$$

□

C Proof of Proposition 3

Proof. Let $g_i = \text{vec}(G_i)$.

Then it holds that

$$\left\| \left(\sum_i^t G_i G_i^\top \right)^{1/2} \right\|^2 = \text{tr} \left(\sum_i^t G_i G_i^\top \right) = \sum_i^t \|G_i\|^2.$$

In the same way,

$$\left\| \left(\sum_i^t G_i^\top G_i \right)^{1/2} \right\|^2 = \sum_i^t \|G_i\|^2.$$

Then we have

$$\left\| \left(\sum_i^t G_i G_i^\top \right)^{1/2} \otimes \left(\sum_i^t G_i^\top G_i \right)^{1/2} \right\|^2 = \left\| \left(\sum_i^t G_i G_i^\top \right)^{1/2} \right\|^2 \left\| \left(\sum_i^t G_i^\top G_i \right)^{1/2} \right\|^2 = \left(\sum_i^t \|G_i\|^2 \right)^2.$$

Let μ denote the mutual the coherence of gradients $\mu = \max_{i \neq j} |g_i^\top g_j| / \|g_i\| \|g_j\|$. Then

$$\left\| \sum_i^t g_i g_i^\top \right\|^2 = \sum_i^t \sum_j^t (g_i^\top g_j)^2 = \sum_i^t \|g_i\|^4 + \sum_i^t \sum_{j \neq i}^t (g_i^\top g_j)^2 \leq \sum_i^t \|G_i\|^4 + \mu^2 \sum_i^t \sum_{j \neq i}^t \|G_i\|^2 \|G_j\|^2.$$

Finally,

$$\left\| \left(\sum_i^t G_i G_i^\top \right)^{1/2} \otimes \left(\sum_i^t G_i^\top G_i \right)^{1/2} \right\|^2 - \left\| \sum_i^t g_i g_i^\top \right\|^2 \geq (1 - \mu^2) \sum_i^t \sum_{j \neq i}^t \|G_i\|^2 \|G_j\|^2.$$

□

D Proof of Proposition 4

Proof. Let $G = U \Sigma V^\top$ be SVD of G . Applying rearrangement, we have

$$\|\text{vec}(G) \text{vec}(G)^\top - L \otimes R\| = \|G \otimes G - \text{vec}(L) \text{vec}(R)^\top\| = \|(U \otimes U)(\Sigma \otimes \Sigma)(V \otimes V)^\top - \text{vec}(L) \text{vec}(R)^\top\|$$

The largest singular value of $G \otimes G$ is σ_1^2 , the corresponding eigenvectors are $u_1 \otimes u_1$ and $v_1 \otimes v_1$. Then the best rank-1 approximation of $G \otimes G$ is

$$\text{vec}(L) \text{vec}(R)^\top = \sigma_1^2 (u_1 \otimes u_1)(v_1 \otimes v_1)^\top.$$

If we reshape, $L \otimes R = \sigma_1^2 (u_1 u_1^\top) \otimes (v_1 v_1^\top)$. So $L = \sigma_1 u_1 u_1^\top, R = \sigma_1 v_1 v_1^\top$ is the solution of the minimization problem. □

E Proof of Proposition 5

Let $\tilde{F} = (Q_A \otimes Q_B)^\top F (Q_A \otimes Q_B)$. Similarly, define $\tilde{E} = (Q_A \otimes Q_B)^\top E (Q_A \otimes Q_B)$. Because of the unitary invariance of the Frobenius norm we have

$$\|\text{diag}(F)\|_F^2 + \|\text{off}(F)\|_F^2 = \|\text{diag}(\tilde{F})\|_F^2 + \|\text{off}(\tilde{F})\|_F^2.$$

Swapping parts of the equation, we finally obtain

$$\|\text{diag}(\tilde{F})\|_F^2 - \|\text{diag}(F)\|_F^2 = \|\text{off}(F)\|_F^2 - \|\text{off}(\tilde{F})\|_F^2 \geq 0.$$

F Ablation Studies

F.1 Performance evaluation

In this section we report the asymptotics of projector-splitting algorithms we use and describe the theoretical overhead of our method. Our approach to dynamically update L_t, R_t by given G_t , described in Algorithm 2 requires 6 matrix-matrix multiplications, 5 scalar product operations (e.g matrix normalization or Frobenius scalar product of two matrices) in comparison with 2 matrix multiplications in the case of Shampoo optimizer. At the first glance it may seem that we need more normalizations in Algorithm 2, but we can omit normalization of L_t and R_t at first two steps and make normalization only at steps 3 and 4 of the algorithm. In the case when we aim to preserve rank-1 approximation of the second Adam moment (`rank1_second_moment = True`), our computational overhead equals to 4 matrix-vector multiplications and 5 vector operations (e.g normalization or scalar product). In practice such an increase in the number of operations does not play a vital role in the overall wall time, but increases it up to 20%. Additionally, we measure the wall time of the fine-tuning of Qwen3-8B on LLM fine-tuning benchmarks (see Table 5).

Table 5: Wall-clock runtime (minutes) for Qwen3-8B fine-tuning across standard LLM benchmarks. All runs use identical hardware, dataloader, and evaluation protocols.

Method	MathQA	GSM8K	HellaSwag	BoolQ	ARC	AVG
SOAP	83	84	87	85	86	85
DyKAF	106	107	109	106	107	107

F.2 Ablation on `rank1_second_moment`

We ablate the effect of enabling the `rank1_second_moment` flag in Algorithm 3, corresponding to a low-rank approximation $V \approx V_L V_R^\top$ of the Adam second-moment matrix V . This approximation reduces memory overhead and, as shown below, may also yield quality improvements depending on the regime. Hyperparameters follow the same tuning protocol as in the main experiments (see Appendix G.1 and Appendix G.2).

Fine-tuning. Table 6 reports results on LLM downstream datasets. The rank-1 approximation generally performs on par with the full-rank update and in some cases yields small improvements, while in others it is slightly worse. This confirms that in fine-tuning regimes—where gradients are often low-rank—the approximation provides memory savings and can be competitive in quality, similar to how parameter-efficient methods such as LoRA may outperform or match full fine-tuning (Veprikov et al., 2025).

Table 6: Ablation study of the rank-1 second moment on LLM fine-tuning benchmarks (Qwen3-8B). Best values are bold.

Method	MathQA	GSM8K	HellaSwag	BoolQ	ARC	ALL
DyKAF (<code>rank1_second_moment=True</code>)	47	39	70	67	85	61.6
DyKAF (<code>rank1_second_moment=False</code>)	45	35	70	70	87	61.4

Pretraining. In contrast, Figure 3 shows that for LLaMA-124M pretraining on FineWeb, the rank-1 approximation increases validation loss across training, confirming that pretraining benefits from a full-rank second moment.

Summary. Overall, the ablation indicates that the `rank1_second_moment` flag is beneficial in fine-tuning scenarios, where gradients tend to be low-rank and the approximation can reduce memory cost while sometimes improving generalization. In contrast, for large-scale pretraining, where gradient structure is richer, the full-rank second moment consistently provides better or more stable performance. We therefore recommend enabling the rank-1 approximation in fine-tuning tasks, but disabling it in pretraining.

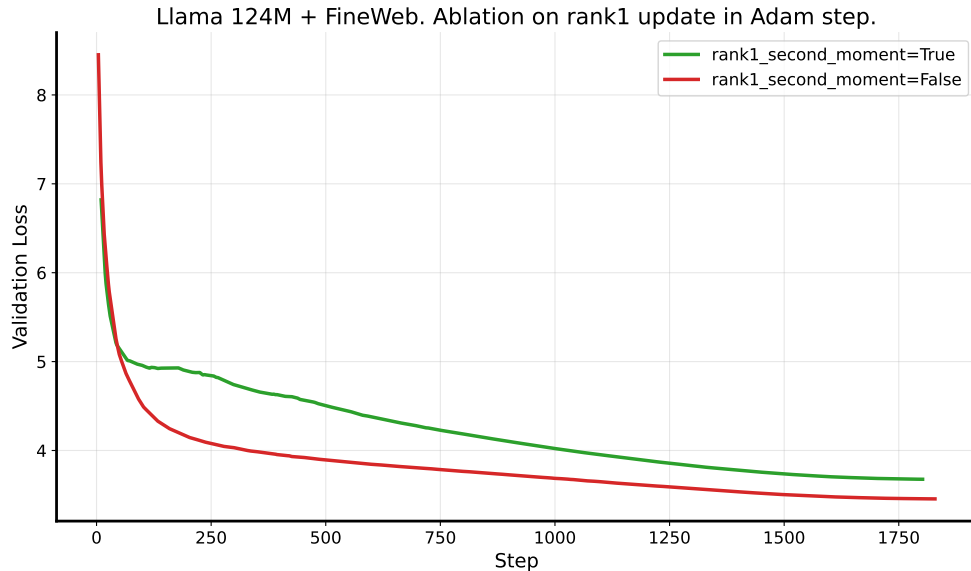


Figure 3: Ablation on `rank1_second_moment` during pretraining of LLaMA-124M on FineWeb. Unlike in fine-tuning, the rank-1 approximation consistently degrades performance, supporting the use of a full-rank second moment in pretraining.

G Experimental Setups and Hyperparameters

G.1 Fine-tuning Experiment (Section 6.1)

Table 7: GLUE full fine-tuning: training setup and hyperparameter sweep.

Parameter	Value
Hardware	RTX-2080 GPU 11GB
Backbone	Roberta-Large (185M)
Trainable params	Self-attention matrices (<code>query_proj</code> , <code>key_proj</code> , <code>value_proj</code>)
Fine-tuning	Full FT (no adapters)
Batch size	16
Grad. accumulation	2
DType	bfloat16
Num train epochs	3 for MNLI, SST-2, QQP, QNLI ; 10 for CoLA, RTE, MRPC
Max seq length	256
Weight decay	1×10^{-6}
Adam parameters	$\beta_1 = 0.9, \beta_2 = 0.999, \varepsilon = 10^{-8}$
LR scheduler	linear, warmup ratio 0.1
Sweep LRs	$\{10^{-5}, 10^{-4}, 5 \times 10^{-4}, 10^{-3}, 5 \times 10^{-3}, 10^{-2}\}$
Update frequency (for SOAP and DyKAF)	10
max evaluation samples	-1 (all evaluation dataset was used)

Table 8: LLM fine-tuning with Qwen3-8B: training setup and hyperparameter sweep.

Parameter	Value
Hardware	A100 GPU 40GB
Backbone	Qwen3-8B
Trainable params	Self-attention matrices (q_proj, k_proj, v_proj, o_proj)
Fine-tuning	LoRA (rank $r=8$, scaling $\alpha=32$, dropout $p = 0.05$)
Batch size	4
Grad. accumulation	1
DType	bfloat16
Max train steps	3000
Max seq length	1024
Weight decay	1×10^{-6}
Adam parameters	$\beta_1 = 0.9, \beta_2 = 0.999, \varepsilon = 10^{-8}$
LR scheduler	linear, warmup 100 steps
Sweep LRs	$\{10^{-6}, 10^{-5}, 5 \times 10^{-5}, 10^{-4}, 5 \times 10^{-4}, 10^{-3}\}$
Update frequency (for SOAP and DyKAF)	10
max evaluation samples	100

Notes. Batch size and maximum sequence length were chosen to fit the available hardware. The number of training epochs (GLUE) or maximum training steps (LLM), gradient accumulation, and the learning rate sweep range were selected as a trade-off between runtime efficiency and final model quality. All remaining parameters follow conventional settings commonly adopted in NLP fine-tuning, and were kept unchanged.

G.2 Pre-train Experiment (Section 6.2)

Table 9: GPT-base pretraining (Shakespeare-char, ~ 160 M tokens): training setup and hyperparameter sweep.

Parameter	Value
Hardware	RTX-2080 GPU 11GB
Backbone	GPT-base (character-level)
Dataset	Shakespeare-char (~ 160 M tokens)
Vocabulary size	96
Batch size	32
Grad. accumulation	1
Sequence length	256
Iterations	30000
DType	bfloat16
Dropout sweep	$\{0.05, 0.1, 0.15, 0.2\}$
Weight decay	0.1
Gradient clipping	0.5
Adam parameters	$\beta_1 = 0.9, \beta_2 = 0.999, \varepsilon = 10^{-8}$
LR scheduler	cosine, warmup 1000 steps
Sweep LRs	$\{10^{-5}, 10^{-4}, 10^{-3}, 5 \times 10^{-3}, 10^{-2}\}$
Update frequency (SOAP, DyKAF)	10
<hr/>	
Model dimensions	
0.41M params	n_embd=128, n_head=4, n_layer=2
1.55M params	n_embd=256, n_head=4, n_layer=2
3.24M params	n_embd=256, n_head=4, n_layer=4

Table 10: Large-scale LLaMA pretraining (FineWeb, ~ 100 B tokens): training setup.

Parameter	Value
Hardware	A100 GPU 80GB
Backbone	LLaMA-124M
Dataset	FineWeb (~ 100 B tokens)
Batch size	32
Gradient accumulation	1
Sequence length	512
Scheduler	Cosine, warmup 3000 steps
DType	bfloat16
Dropout	0.0
Weight decay	0.1
Grad. clipping	0.5
Adam parameters	$\beta_1 = 0.9, \beta_2 = 0.999, \varepsilon = 10^{-8}$
LR	10^{-3}
Update frequency (SOAP, DyKAF)	10
Model dimensions	n_embd=768, n_head=12, n_layer= 12

Notes. Most hyperparameter choices in pretraining follow the same principles as in the fine-tuning experiments (Appendix G.1): hardware-constrained batch size and context length, training steps set as a trade-off between runtime and quality, and otherwise conventional settings adopted in large-scale pretraining. For DyKAF we used the full-rank second moment (`rank1_second_moment = False`), consistent with our observation that pretraining benefits from richer curvature estimates. Importantly, in the large-scale LLaMA-124M FineWeb run (Table 4) we did not perform any hyperparameter tuning for DyKAF, instead reusing SOAP settings directly. This highlights the robustness of DyKAF to hyperparameter choices even under resource-intensive training regimes.

H Higher Order Projector-splitting

We can generalize Kronecker Fisher approximation to tensor-shaped parameters. Let the gradients G_i be tensors of shape $n_1 \times n_2 \times \dots \times n_d$. The Fisher matrix is defined the same way as in matrix case:

$$F_t = \sum_i \text{vec}(G_i) \text{vec}(G_i)^\top.$$

We aim to solve the nearest Kronecker approximation problem:

$$\|F_t - L_t^{(1)} \otimes L_t^{(2)} \otimes \dots \otimes L_t^{(d)}\| \rightarrow \min_{L_t^{(1)}, \dots, L_t^{(d)}},$$

where $L_t^{(k)} \in \mathbb{R}^{n_k \times n_k}$, using projector-splitting.

Let $G_t^{(k)} \in \mathbb{R}^{n_k \times (n_1 \dots n_{k-1} n_{k+1} \dots n_d)}$ denote the unfolding (rearrangement) of tensor G_t into a matrix by the k -th dimension.

The following algorithm is an adaptation of projector-splitting (Ceruti et al., 2022, Section 4) for the nearest Kronecker approximation of Fisher matrix in case of tensor-shaped parameters.

Algorithm 5 `kron_proj_split` for tensors. Dynamical Kronecker approximation of Fisher matrix.

Require: $\{L_t^{(i)}\}_{i=1}^d \in \mathbb{R}^{n_i \times n_i}$ – Kronecker product approximation of the Fisher matrix on the optimization step t , $G_t \in \mathbb{R}^{n_1 \times n_2 \times \dots \times n_d}$ – gradient with respect to the layer W_t .

- 1: **for** $k = 1 \dots d$ **do**
 - 2: $\text{norm}_k = \left\| L_t^{(1)} \right\|_F \dots \left\| L_t^{(k-1)} \right\|_F \left\| L_t^{(k+1)} \right\|_F \dots \left\| L_t^{(d)} \right\|_F$
 - 3: $\hat{L}_t^{(k)} = L_t^{(k)} \text{norm}_k^2 + G_t^{(k)} \left(L_t^{(1)} \otimes \dots \otimes L_t^{(k-1)} \otimes L_t^{(k+1)} \otimes \dots \otimes L_t^{(d)} \right) G_t^{(k)\top}$
 - 4: $L_{t+1}^{(k)} = \hat{L}_t^{(k)} / \left\| \hat{L}_t^{(k)} \right\|_F$
 - 5: $S = \prod_k \langle L_t^{(k)}, L_{t+1}^{(k)} \rangle_F + \text{vec}(G_t) \left(L_{t+1}^{(1)} \otimes \dots \otimes L_{t+1}^{(d)} \right) \text{vec}(G_t)^\top$
 - 6: **return** $\{S^{1/d} L_{t+1}^{(k)}\}_{i=1}^d$.
-